Impact of Separator's Solid-Phase Ion Conductivity Parameter on Convection Battery Performance and Modeling

Ramsey Hilton, Michael Gordon, Donald Dornbusch, and Galen J. Suppes
Dept. of Chemical Engineering, University of Missouri-Columbia, Columbia, MO 65211

DOI 10.1002/aic.14568
Published online August 1, 2014 in Wiley Online Library (wileyonlinelibrary.com)

A solid-phase ion conductivity parameter has been added to the separator of a porous electrode theory description of a convection battery performance to increase the accuracy of this model. With the addition of the ion conductivity parameter, the variances between the model and experimental data have been reduced by 80–85% in both the convection cell and the diffusion cell. The parameter is fundamentally consistent with solid-phase mechanisms by which ions can transport through separators in parallel with liquid-phase transport, and the improved modeling results substantiate the importance of solid or surface ion transport mechanisms at high current fluxes. Modeling was supplemented with dimensionless analysis to lump fundamental parameters that are inherently coupled in the underlying equations. From this analysis, a global parameter has been developed describing the ratio of convective charge transfer to diffusive charge transfer that characterizes the transition from diffusive to convective cell behavior. © 2014 American Institute of Chemical Engineers *AIChE J*, 60: 3784–3791, 2014
Keywords: electrochemistry, electronic materials, diffusion (in membranes), energy

Introduction

The pumps of lithium iron phosphate convection cells force liquid electrolyte through flow cells to reduce concentration overpotentials.[1] This improvement has been evident in multiple battery chemistries.[2–4] In laboratory experiments, this approach has been effective to substantially reduce charge times and eliminate dendrite modes of failure with cycled lithium metal anodes.

The key difference between a convection battery and a flow battery lies in the electrolyte. A flow battery has two electrolyte solutions, and they are kept separate, in order to prevent mixing of reactive species[5,6]—ion flow though the separator and between counter-electrodes is limited by diffusive and migration forces. Convection batteries involve only one electrolyte that flows from one electrode to the counter electrode. Battery chemistries used in flow batteries are not compatible with the convection battery configurations while the vast majority of conventional battery chemistries are compatible with the convection battery. Figure 1 is a visual representation of the differences between these two cell types.

A fairly robust predictive model was developed by Gordon and Suppes[7]; it modeled cell voltage vs. time, cell capacity, overpotentials in the separator, and concentration of Li^+ ions throughout the cell. This model uses porous electrode theory as developed by Newman et al.[8,9] The major advantage of this model is its ability to qualitatively display the behavior of Li^+ ions in all four regions of the cell (negative electrode, separator, positive electrode, and tubing) including the impact of electrolyte flow rate. These modeling efforts were able to quantify how electrolyte flow leads to the elimination of bulk diffusion limitations in batteries. Insight into the concentration gradients set the foundation for an approach to eliminate dendrite modes of failure.[10] The highest velocity modeled (118 μm/s, equal to the experimental velocity) gave way to minimal fluctuation in the concentration of the Li^+ ions throughout the cell.

Although the model was qualitatively accurate, a shortcoming of this model was its inability to quantitatively predict realized capacity over a wide range of current densities. A hypothesis was put forward that solid-phase transport of counterions in the separator (see Figures 2 and 3 illustrations) was a rate-limiting mass-transfer mechanism in the convection battery that was necessary to maintain electroneutrality. This article is on the testing of this hypothesis through modeling efforts with a revised model and theory that includes solid-phase transport of ions in the separator.

Model Derivation

Previous works have shown that convective flow can increase the current density by a factor of 6 relative to no-flow conditions under the constraint of a constant realized amp-hour capacity from the battery. At higher flow rates, a mass balance around the cathode indicates that the current is equal to the volumetric flow rate of the electrolyte times ΔC_{Li^+} where delta is the difference between entering and exiting concentrations. To maintain charge neutrality in solution, an equivalent amount of lithium's counter-anion must leave the control volume. The following constraints apply:

Correspondence concerning this article should be addressed to R. Hilton at rhwv9@mail.missouri.edu.

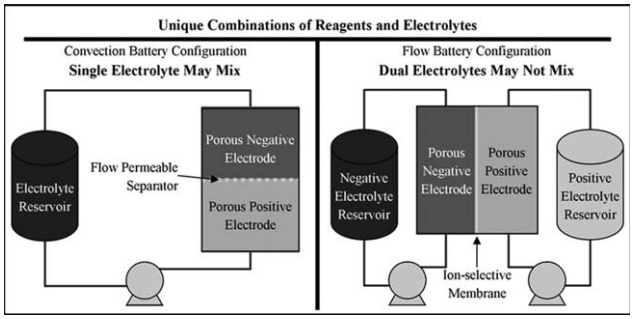

Figure 1. Visual depiction of contrast between flow battery and convection battery.[7]

- The large distances of the tubing (connected to pump), both diffusion and migration of the anion through the tubing would tend to be negligible
- Typically low cross-sectional area of the separator open to flow

A primary mechanism for counter-anion must be either through the plastic/solid part of the separator or along the pore (flow channels) surfaces of the separator. The need for this solid-phase-coupled mechanism is particularly exasperated at the higher current densities of the convection battery.

Figures 2 and 3 illustrate this transport both in terms of illustrations and equations. Equations are derived for the case where the separator is treated as a pseudohomogeneous phase. A key artifact sought for elucidation is whether or not the pseudohomogeneous model is able to distinguish between solid and liquid transport.

As seen by the mass-transfer equation (Figure 2), the solid- and liquid-phase diffusivities appear as $D_{1\text{eff}}$ and $D_{2\text{eff}}$, respectively. In this form, the COMSOL software cannot distinguish between the solid- and liquid-phase diffusivity values; in other words, the solid-phase and liquid-phase effective diffusivities cannot be decoupled.

However, for the current flux equation of Figure 3, the ion conductivities ($K_{1\text{eff}}$ and $K_{2\text{eff}}$, respectively) can be decoupled. The ion conductivities can be decoupled because the transference numbers depend on the properties of the liquid/solid, and the solid phase of the separator will have a different transference number than the liquid phase.

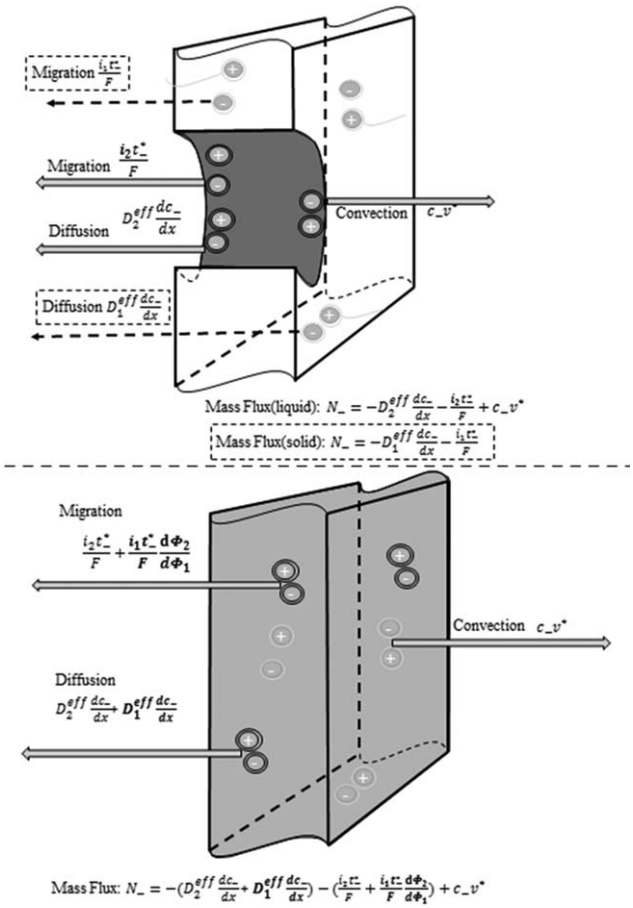

Figure 2. Illustration of solid-phase ion flux, occurring separately from liquid-phase ion transport as it happens in theory (top), and how the model treats liquid- and solid-phase ion as a pseudosingle phase (bottom).

Terms in dotted boxes represent solid-phase transport terms not previously accounted for in the model. Bold terms are the terms added to the new model with the pseudosingle phase.

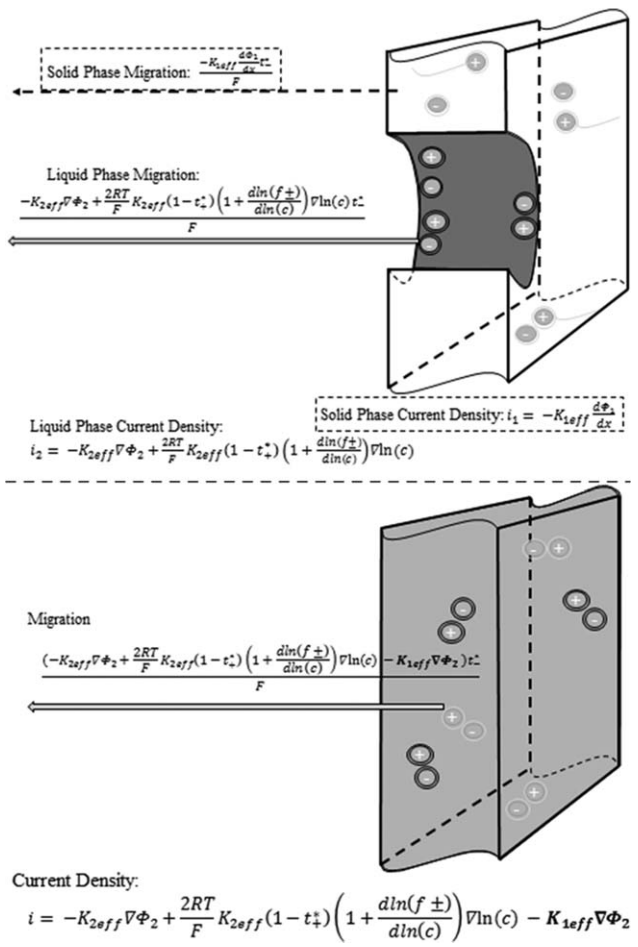

Figure 3. Representation of migration term of solid-phase ion flux, treated separately from liquid phase (top) and treated as a pseudosingle phase (bottom).

Although the summarizing equation of Figure 2 is a mass-transfer equation, this figure summarizes in terms of current flux.

The transference numbers (t_+^*, t_-^*) of the positive (Li^+) and negative (PF_6^-) ions refer to the fraction of the total current carried by those ions. The positive transference number (t_+^*, t_-^*) is derived in the following equation

$$t_+^* = \frac{i_+}{i_{\text{tot}}} = \frac{F z_+^2 v_+ c_+}{F^2 \sum_i z_i^2 v_i c_i} \tag{1}$$

Where F = Faraday's Constant (96,485 C/mol)
i_+ is current carried by positive ions (A)
i_{tot} is total current (A)
z_i is the charge of a single ion, C
v_i is the mean molar velocity of a species (m/s)
c_i is the concentration of a species (mol/m^3)

The transference number of a species is related to several factors. First, the size and mobility of an ion can determine how quickly it is able to transfer charge. A smaller ion moves faster, and it also is less stable with a charge, because it has less volume for a charge to be distributed. For this reason, it loses its charge faster than a larger ion. In addition to the ions, the transference number is also dependent on the media through which the charge transfer is occurring. A medium with small pores is more conducive to charge transfer with smaller ions. In this specific cell, Li^+ is a much smaller ion than PF_6^-, so the t_+^* value should be greater in the solid phase than it is in the liquid phase, because the smaller ion flows more freely in the solid porous phase than the larger ion, where they both flow freely throughout the liquid phase. For this reason, transference numbers are regional parameters, changing from one medium to another within the cell, but they are regarded as global constants in this model.

The conclusion from the analysis of this model is that the representation of the two phases of the separator as a pseudohomogeneous phase will allow, to some extent, the impact of the solid-phase transport to be decoupled from the impact of the liquid-phase transport even though they are lumped into the same equations.

For the model/derivation as presented, the solid phase is modeled in the extreme case where only the anion is mobile. This representation is the manifestation of the case where the solid phase of the separator is an ion exchange media where the positive ion is immobile. The fact is that what is presented as a solid-phase transport could actually be any transport that is independent of the bulk liquid transport including the exemplified ion exchange media mechanism and also including surface (liquid–solid interface) transport mechanisms.

Although solid-phase conductivity parameters are often included in the modeling of electrodes, previous porous electrode theory work has not included a solid phase (ion) conductivity of the separator. Ion conductivity is to be distinguished from electron conductivity as the current of ion transport is coupled with the mass-transfer equations and limitation.

The following equations, derived from Newman and Thomas-Alyea,[11] describe the liquid-phase and solid-phase current densities, respectively

$$i_2 = -K_{2\text{eff}} \nabla \Phi_2 + \frac{2RT}{F} K_{2\text{eff}} \left(1 - t_+^*\right) \left(1 + \frac{d \ln(f\pm)}{d \ln(c)}\right) \nabla \ln(c) \tag{2}$$

$$i_1 = -K_{1\text{eff}} \frac{d\Phi_1}{dx} \tag{3}$$

The most crucial addition to the model is in the separator region, and it is a solid-phase ion conductivity term, $K_{1\text{eff}}$. Within the separator, the improvement in overall current brought on by a solid-phase conductivity term can be applied by adding the solid-phase current density term to the liquid-phase current density term. The following equation applies in the separator, in which i is total current density

$$i = -K_{2\text{eff}} \nabla \Phi_2 + \frac{2RT}{F} K_{2\text{eff}} \left(1 - t_+^*\right) \times \left(1 + \frac{d \ln(f\pm)}{d \ln(c)}\right) \nabla \ln(c) - K_{1\text{eff}} \nabla \Phi_1 \tag{4}$$

As shown in Figures 2 and 3, the model applies the solid-phase conductivity term within a pseudosingle phase. This both accounts for solid-phase ionic conductivity in the separator, and model converges properly with this application. The following equation applies

$$i = -K_{2\text{eff}} \nabla \Phi_2 + \frac{2RT}{F} K_{2\text{eff}} \left(1 - t_+^*\right) \times \left(1 + \frac{d \ln(f\pm)}{d \ln(c)}\right) \nabla \ln(c) \; - K_{1\text{eff}} \nabla \Phi_2 \tag{5}$$

After rearrangements and substitutions, the following equation is derived. $K_{1\text{eff}}$ (showcased in bold) is the solid-phase ion conductivity within the separator, and it is the most important addition to the model

$$(K_{2\text{eff}} + \boldsymbol{K_{1\text{eff}}}) \frac{d^2 \Phi_2}{d^2 x} = \frac{2RT}{F} K_{2\text{eff}} \left(1 - t_+^*\right) \frac{d^2 \ln c}{dx^2} - a i_n \tag{6}$$

Within the separator, the following equations define $K_{1\text{eff}}$ and $K_{2\text{eff}}$

$$\boldsymbol{K_{1\text{eff}}} = K_{1\text{sep}} * \varepsilon_{1\text{sep}}^{\text{Br}} \tag{7}$$

$$K_{1\text{sep}} = K_{1\text{sep}-\text{ionic}} + K_{1\text{sep}-\text{electronic}} \tag{8}$$

In the separator, $K_{1\text{sep}-\text{electronic}}$ is assumed to be negligible, so $K_{1\text{sep}} = K_{1\text{sep}-\text{ionic}}$. As discussed by Park et al.,[12] who derive several equations describing conduction in a lithium battery, solid-phase ion conductivity is directly proportional to solid-phase diffusivity, $D_{1\text{eff}}$. Liquid-phase conductivity and porosity within the separator are described by the following two equations

$$K_{2\text{eff}} = \mathrm{K}_{2\text{sep}} * \varepsilon_{2\text{sep}}^{\text{Br}} \tag{9}$$

$$\varepsilon_{1\text{sep}} + \varepsilon_{2\text{sep}} = 1 \tag{10}$$

Model Parameters

Tables 1 through 3 provide the parameters used to perform the simulation of the lithium iron phosphate battery. The parameters from Table 1 are values for literature. Table 2 are values specifically measured for the materials of study reported here. Table 3 reports the remaining parameters used to complete the simulation—these values were fit to the data with values provided from literature and Gordon and Suppes[7] for comparison. These optimized values were determined by a variation of the method of least squares, in which the parameters were continually manipulated until the deviation between experimental and model data was minimized. The values measured directly have the lowest confidence intervals (highest accuracy), followed by the values from literature, which all have different confidence intervals,

Table 1. Parameters from Literature

Parameter	Value	Units	Description	Source
rp_-	5	μm	Particle radius Negative	10
rp_+	7	μm	Particle radius Positive	10
S_-	18.84	m^2/m^3	Specific surface area Negative	13
S_+	12.7286	m^2/m^3	Specific surface area Positive	13
Brug	1.5		Bruggeman coefficient	13
t_+	0.343		Cationic transport number	13
ε_{1+}	0.297		Solid phase vol-fraction Positive	14
ε_{1-}	0.471		Solid phase vol-fraction Negative	14
ε_{1sep}	1.5		Separator solid volume fraction	14
ε_{2+}	0.444		Electrolyte phase vol-fraction Positive	14
ε_{2-}	0.357		Electrolyte phase vol-fraction Negative	14
ε_{2sep}	5		Separator porosity	13
K_{1+}	3.8	S/m	Solid phase conductivity Negative	13
K_{1-}	100	S/m	Solid phase conductivity Positive	13
k_-	2	μm/s	Reaction rate coefficient Negative	13
k_+	2	μm/s	Reaction rate coefficient Positive	13
α_a	0.5		Apparent transfer coefficient for anodic reaction	13
α_c	0.5		Apparent transfer coefficient for cathodic reaction	13

Table 2. Parameters Measured Directly

Parameter	Value	Units	Description
i_2	Varied	A/m^2	Applied current density
A_{cell}	1.27	cm^2	Cell cross section area
T	298	K	Temperature
L_-	7.0	mm	Length of negative electrode
L_{sep}	0.53	mm	Length of separator
L_+	7.0	mm	Length of positive electrode
L_{tubing}	60	cm	Length of tubing and electrolyte reservoir
c_o	1000	mol/m^3	Initial electrolyte salt concentration
V	118	μm/s	Velocity of electrolyte fluid

depending on the methods used in the cited literature. The highest confidence intervals lie in the optimized values, as these values are modified from earlier accepted values to fit the data.

As indicated by Table 3, the artificial diffusivity parameter was set to zero in this study. This parameter was not identified with a fundamental phenomenon or property and served primarily as a correcting factor. With the addition of the solid-phase conductivity term, the predictive ability of the model is robust without the artificial diffusivity parameter.

Dimensionless Analysis

With over 35 parameters involved in the simulation, the question arises if all of these are truly decoupled/independent in the mass and charge balance equations used to determine analytical solutions. The equations were reduced to a dimensionless form evaluate if the certain of these parameters were systematically coupled in dimensionless numbers. Additionally, this analysis gives way to the ratio of convective to diffusive charge transfer, a dimensionless parameter labeled E_i. Table 4 summarizes dimensionless values of the model parameters derived in a manner similar to that used by Guduru.[16]

Few of the parameters have values that are constant throughout the cell. Each parameter that includes a K^{eff} or a D^{eff} value varies from anode to separator to cathode. Dimensionless parameter A (Eq. 11) where $a=S_i * L_i/L_{cell}$, described in words, is the following

$$\frac{\text{Change slope of the potential within electrolyte with respect to position at a given point within the cell}}{\text{Total charge transfer between solid and electrolyte}}$$

Given that K_{1eff} and K_{2eff} are regional parameters dependent on K_1, K_2, and ε in each region of the cell, A is a parameter that changes from one cell region to another.

A dimensionless parameter B_i (Eq. 12) has the same significance as parameter A, but with total change in electrolyte potential slope throughout the cell added to the numerator.

Table 3. Parameters Optimized to Fit Data

Parameter	Initial Value From Literature	Gordon Paper Value	Optimized Value	Units	Description	Source
C_{o-}	13,070	1700	1700	mol/m^3	Initial solid-phase conc Negative	15
C_{o+}	4,744	100	100	mol/m^3	Initial solid-phase conc Positive	15
C_{1max-}	26,400	2550	2550	mol/m^3	Max solid-phase concentration Negative	15
C_{1max+}	23,720	4860	4860	mol/m^3	Max solid-phase concentration Positive	15
D_2	8E-18	1.00E-11	1.00E-11	m^2/s	Salt diffusivity in electrolyte	14
D_{1-}	5E-9	3.90E-14	8E-11	m^2/s	Solid-phase Li-diffusivity Negative	15
D_{1+}	IE-9	5.00E-10	4E-9	m^2/s	Solid-phase Li-diffusivity Positive	15
K_{1-}	7	3.8	4.7	S/m	Solid-phase electronic conductivity in negative electrode	13
K_{1sep}	Not used	Not used	5	S/m	Solid-phase total conductivity in separator	–
D_{art}	1E-6	1E-6	0	m^2/s	Artificial Diffusivity	13

Table 4. Full List of Dimensionless Parameters

Parameter	Negative	Separator	Positive
A	$A=\frac{(K_1^{\text{eff}}+K_2^{\text{eff}})\frac{d^2\phi_2}{dx^2}}{ai_x}$		(11)
B_i	$\frac{2RT(K_1^{\text{eff}}+K_2^{\text{eff}})\frac{d^2\phi_2}{dx^2}}{F}\left(1-t_i^*\right)\frac{d^2\ln c}{dx^2}$		(12)
I	$\exp\left(\frac{\alpha_a F\eta_s}{RT}\right)-\exp\left(\frac{\alpha_c F\eta_s}{RT}\right)$		(13)
K	$\frac{\text{K2}_{\text{eff}}}{\text{K1}_{\text{eff}}}$		(14)
C_{in}	$\frac{(c_i)^2 s_{\text{neg}}}{\left(\frac{dc_i}{dx}\right)^2 D_2^{\text{eff}} c_0}\frac{dc_i}{dt}$ (15a)	$\frac{(c_i)^2 s_{\text{sep}}}{\left(\frac{dc_i}{dx}\right)^2 D_2^{\text{eff}} c_0}\frac{dc_i}{dt}$ (15b)	$\frac{(c_i)^2 s_{\text{pos}}}{\left(\frac{dc_i}{dx}\right)^2 D_2^{\text{eff}} c_0}\frac{dc_i}{dt}$ (15c)
D_{li}	$\frac{A_{\text{cell}}}{c_i}\frac{d^2 c_i}{dx^2}$		(16)
D_{nsi}	$\frac{D_1^{\text{eff}} c_i}{\left(\frac{d^2 c_i}{dr^2}+\frac{1}{r}\frac{dc_i}{dr}\right)*\left(D_1^{\text{eff}}+D_2^{\text{eff}}\right)}$		(17)
E_i	$\frac{c_i * v^*}{\left(D_1^{\text{eff}}+D_2^{\text{eff}}\right)\frac{dc_i}{dx}}$		(18)
H_i	$H_i=\frac{D_2^{\text{eff}}}{L_{\text{cell}}}\frac{F}{(1-t_i^*)a*i_x}\frac{dc_i}{dx}$		(19)
F_i	$\frac{N_i L_{\text{cell}}}{c_0 D_2^{\text{eff}}}$		(20)
G_i	$\frac{i_2 t_i^*}{F}\frac{L_{\text{cell}}}{c_0 D_2^{\text{eff}}}$		(21)
Ji	$\frac{cv^* L_{\text{cell}}}{c_0 D_2^{\text{eff}}}$		(22)
L_i	$\frac{L_{\text{cell}} 2RT(K_1^{\text{eff}}+K_2^{\text{eff}})t_i(1-t_i)}{c_0 D_2^{\text{eff}} F^2}\frac{1}{c}\frac{dc}{dx}$		(23)
M_i	$\frac{t_i^* L_{\text{cell}}(K_1^{\text{eff}}+K_2^{\text{eff}})}{Fc_0 D_2^{\text{eff}}}\frac{d\Phi_2}{dx}$		(24)
N_i	$\frac{(1-t_i^* a*i_x)c_i^2}{D_2^{\text{eff}} Fc_0\left(\frac{dc_i}{dx}\right)^2}$		(25)

This parameter is also regional and changes as $K_{1\text{eff}}$ and $K_{2\text{eff}}$ change throughout the cell.

A dimensionless parameter I (Eq. 13) is the ratio of the charge transferred between the solid and the electrolyte and the exchange current density. This parameter is taken directly from the Butler–Volmer equation (Eq. 26)

$$i_0=k_i(c_{1\max-i}-c_i)^{\alpha_a}(c_i)^{\alpha_c}(c)^{\alpha_a} \tag{26}$$

K (Eq. 14) is the ratio of the effective conductivity within the electrolyte to that in the solid. It describes the ratio of the resistance (voltage drop) within the solid to the voltage drop within the electrolyte.

C_{in} is a ratio of charge transfer brought on by changes in concentration over time to charge transfer from the applied current to the system. The i subscripts denote that this parameter can be applied to both anions and cations. This is a regional parameter because ε changes from anode to separator to cathode.

D_{li} applies to the electrolyte and is used for the liquid-phase material balance. It is somewhat similar to parameter C_n. This is a ratio of charge transfer brought on by changes in the slope of concentration with respect to position in the cell to charge transfer brought on by applied current to the system.

D_{si} is the same as D_{li} but it applies to the solid phase. D_{si} is dependent on solid particle radius in the positive electrode (rp_+) while D_{si} is dependent on the solid particle radius of the negative electrode (rp_-).

E_i (Eq. 18) is a ratio of convective charge transfer to diffusive charge transfer in this system, which can also be defined as the Sherwood number of the electroactive species. The rate of convective charge transfer is dictated by the flow velocity of the electrolyte solution through the convection cell, the size of the cell, and the concentration gradient of charged particles across the cell. The diffusive charge transfer in the denominator is similar to the quantity discussed by Daum and Murray,[17] who discuss diffusive charge transfer and its dependence on a concentration gradient of charged particles across a membrane. This is a ratio that can have broader impacts in the modeling of batteries in the future. A more general definition of this dimensionless number in a convection cell can be defined by Eq. 18a

$$E=\frac{vc}{D\frac{dc}{dx}} \tag{18a}$$

Where:

v = flow velocity of electrolyte solution (m/s)

D = diffusivity of electroactive species between solid particles and electrolyte solvent (m^2/s)

c = anion/cation concentration at a given point within the cell (mol/m^3)

dc/dx = change in salt concentration in the axial direction along the cell (mol/m^4)

Dimensionless forms of diffusion and migration are expressed by parameters H_i and F_i. These are simplified to F_i, G_i, and J_i (Eqs. 20–22) as dimensionless parameters used to define the ion flux equation.

Equations 27–30 provide the dimensionless liquid- and solid-phase charge balances and dimensionless liquid- and solid-phase material balances, respectively

$$A=B-1 \tag{27}$$

$$A=IK \tag{28}$$

$$C_n=D_{\text{li}}-E_i+N_i \tag{29}$$

$$\text{C}_n=\text{D}_{\text{s}n} \tag{30}$$

The i subscript indicates that the parameter applies to the anion and the cation. The ion flux of a given species is described by Eq. 31

$$H_i=-F_i+G_i-J_i \tag{31}$$

L_i and M_i (Eqs. 23 and 24) relate net current transported by liquid to the different overpotentials of the cell. Equation

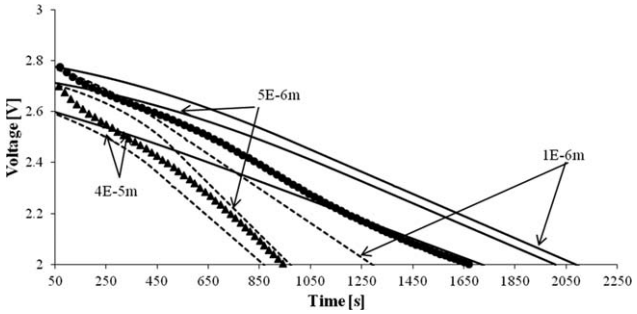

Figure 4. Experimental (flow = circles, no flow = triangles) and modeled (flow = solid, no flow = dashed) voltage curves at several negative electrode particle radii (46.9 A/m^2).

Particle radii are variesd between 1E-6m, 5E-6m, and 4E-5m. The last 25% of each model profile is extrapolated based on trends due to model convergence difficulties as the capacity of the battery diminishes.

32 describes how the aforementioned parameters to describe the net current of the system in a binary electrolyte

$$G_i = -M_i + L_i \tag{32}$$

Simulation Results

The convection battery performance is compared to porous electrode theory modeling results in the following sequence to evaluate the extent to which the model accurately represents performance:

- A typical voltage-time profile at high load is evaluated as a function of negative electrode particle size.
- Cell capacity evaluated as a function of $K_{1\text{eff}}$.
- Voltage-distance profiles in the positive electrode are evaluated relative to a reference electrode.

The voltage-time profiles of Figure 4 show that particle diameter of the negative electrode has a significant impact on both the profile and realized capacity. The following observations were used to correlate actual performance with model projections.

- The cell's voltage profiles exhibit inflection points at about 300 s which can be attributed to the end of non-Faradaic capacitance which the Butler–Volmer model is not able to simulate. No attempt is made to fit the model to the first 300 s of the voltage profiles.
- Initial model voltages are a function of the particle size which is not a characteristic of the actual cell voltage profiles, and so, no attempt was made to match the model with the cell profile for the first 300 s.
- The experimental cells exhibit an initial drop in voltage, due to an inherent capacitance in the electrode particles and immediate release at the beginning of closed circuit time, not yet accounted for mathematically in the model.
- The model consistently projects high voltages with convective flow vs. diffusion alone.
- The model consistently projects that larger particles will exhibit lower voltages and low realized capacities at this constant current simulation.
- The optimal fit is at diameters of about 4E-5 m with both the convective flow and nonconvective flow having reasonable fits at this particle size. The optimal fit was based on both the voltage profile (after 300 s) and the total mA-h capacity realized until reaching the lower cutoff voltage.

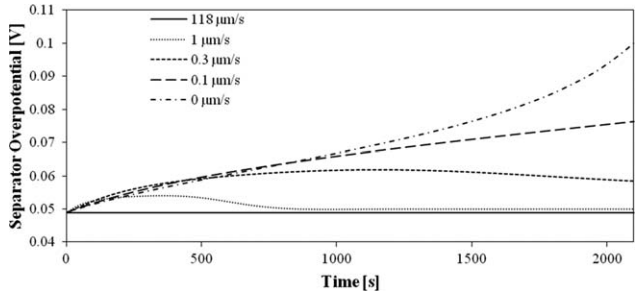

Figure 5. Concentration overpotential in separator as a function of flow velocity.[7]

The modeled voltage behavior summarized by Figure 4 is consistent with the experimental findings of Sun et al.[18] as well as the findings of this study.

The model provides valuable insight into how flow and thicker electrodes (7 mm) impact battery performance. Flow allows the active components of the electrode near the surface of the particles to be realized for the entire depth of the electrode while the nonflow case is limited by diffusion overpotentials for the particles located further from the separator (more-rapid voltage drop with time). This interarticle bulk (liquid) diffusion overpotential was summarized by Gordon et al. as provided by Figure 5.

Increasing velocities within the convection cell lead to reduced concentration gradients. This leads to substantially reduced separator overpotentials up to the point where the overpotential of Li^+ is eliminated and only the overpotential associated with the anion migration/diffusion remains (Figure 5). The lower overpotentials with increasing velocities (Figure 5) are consistent with the voltage curves from Figure 4.

A primary purpose of the modeling effort of this article is to evaluate the impact of using a solid-phase ion conductivity parameter in the separator, $\mathbf{K_1}$, to improve the model representation of the experimental data. Figure 6 shows contour lines for various values of this new parameter.

The contour line for $\mathbf{K_1} = 0$ corresponds to a further optimization of the parameters as summarized in Table 3. The new

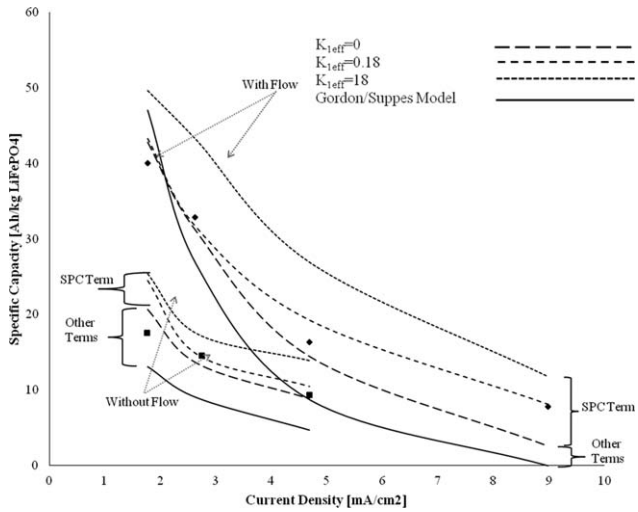

Figure 6. Specific capacity model improvements from changed terms.

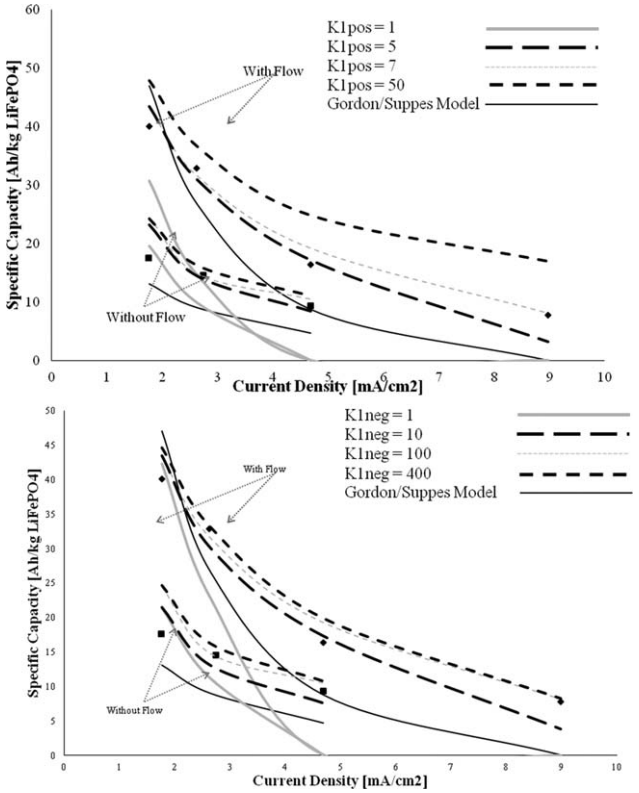

Figure 7. Variations of electrode conductivity values(K_{1eff} in separator set to 0.18).

parameters tend to between the values of Gordon and Suppes and those otherwise reported in literature. The fit is substantially improved just by these parameters; however, at current densities >4 mA/cm^2, the optimized parameters are not enough to accurately represent the data. At a value of $\mathbf{K_1} = 0.18$, the model accurately represents the convection battery performance including performance at >4 mA/cm^2. The solid-phase conductivity parameter improves the fit to the data. Also, this modeling effort illustrates how the solid-phase conductivity parameter has an important role for realizing higher values of current density, especially values >10 mA/cm^2.

Figure 7 summarizes the impact of the solid-phase ionic conductivity parameter in the positive and negative electrodes. There is generally a greater sensitivity of the modeled to values of the positive electrode conductivity. It is possible that the model if more sensitive to solid-phase cation conductivity in the electrodes and solid-phase anion conductivity in the separator.

From the convection cell data (with flow), the average variance between the model data and the experimental data decreases by 65% when the new values are assigned to the diffusivities and the positive electrode conductivity terms. When these new values are assigned along with the addition of the solid-phase conductivity term in the separator, the variance between the experimental and model data reduces by an average of about 84%. For the diffusion cell data, the average variance reduces by about 80% for both the application of the new terms with and without the new solid-phase conductivity term.

The model yields higher capacities at each current density with the solid-phase conductivity term applied. The addition of the solid-phase conductivity term in the separator and the

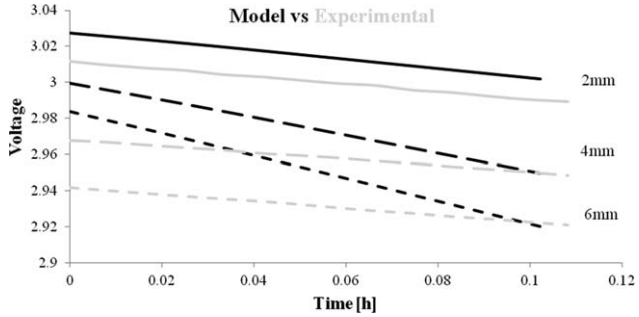

Figure 8. Comparison of model and experimental reference electrode voltage slopes at different distances from cathode current collector.

manipulation of a few key parameters, this model is becoming more useful for quantitative predictions of battery performance. This parameter has the fundamental significance as summarized by Figures 2 and 3.

The model of the convection cell is able to report voltages as function of distance from the cathode current collector in the positive electrode. Figure 8 compares model and experimental voltage profiles depths of 2, 4, and 6 mm. There is good qualitative agreement and further verification of the model accuracy.

Discussion

This article has presented further-optimized modeling results using porous electrode theory as applied to a convection battery and with the introduction of a solid-phase ion conductivity parameter to the separator. In a porous environment, it is possible for convection of a Li-Ion chemistry to provide bulk Li^+ with near-zero overpotential losses with the anion conductivity of the separator playing a key role for maintaining electroneutrality in the electrolyte. When presented in dimensionless form, the new parameter, $E+$, provides a ratio of convective to diffusive mass transfer believed to be representative of Li^+ transport. Figure 8 displays the average value of the dimensionless number $E+$ (see Eq. 18) within the separator as a function of flow velocity.

In the separator, as velocity increases dc/dx simultaneously decreases. At high velocities, dc/dx is essentially zero.[7] $E+$ increases by at least two orders of magnitude for each order of magnitude increase in the velocity. Figure 9 illustrates how even low velocities allow convective transport to overwhelm diffusive contributions. It also outlines the effect

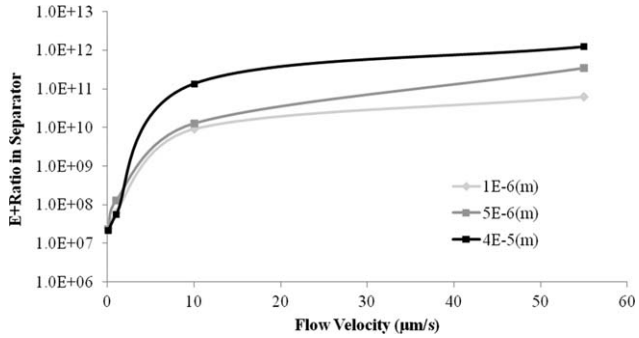

Figure 9. Average $E+$ value within separator vs. flow velocity (middle of discharge time), simulated at multiple negative electrode particle sizes.

of particle size on the $E+$ ratio, particularly at the higher flow velocities. At the higher velocities, the higher particle diameters yield a higher $E+$ ratio. Larger particles are less conducive to interparticle diffusion, which makes convective charge transfer a more dominant force throughout the cell, even in the separator. At the lower velocities, the particle size does not have as great of an impact on this ratio, as concentration gradients within the particles are not as pronounced, and the particles can be treated as lump systems.

This dimensionless value, E, can have broader impacts, as it can indicate whether convection or diffusion are the dominant driving forces during specific times of charge/discharge and at specific points throughout the cell. Based on this ratio, adjustments can be made to a cell's design to optimize performance and availability of charged species to be transferred. For example, if convective charge transfer dominates in a specific region of the cell, the diffusive charge transfer can be improved using a higher surface area electrode powder or separator in that region. If diffusive charge transfer dominates throughout the cell, flow velocity can be increased.

Conclusions

Porous electrode theory relies on over 36 parameters, the optimization of which can be overwhelming. This work demonstrated that a focus on diffusivities and solid-phase ion conductivities can yield significant model improvement. Both a theoretical foundation and practical need for a solid-phase ion conductivity were demonstrated—this parameter is especially important for performances at high current fluxes in the convection battery. Previously used artificial diffusivity parameters provided no value in this model and may be more-appropriately replaced with the solid-phase ion conductivity of the separator. This is especially the case as the latter has a fundamental basis.

The solid-phase conductivity parameter is constructed in the same way as the liquid-phase conductivity parameter with local solid conductivity, porosity of solid, and Bruggeman coefficient. The application of the manipulated parameters along with the addition of the solid-phase conductivity parameter reduces the variance between experimental and model specific capacity by 80–85% for both the diffusion cell and convection cell data.

A dimensionless parameterization of the porous electrode model has been derived. A dimensionless ratio of convective to diffusive charge transfer effectively demonstrates how even low velocities can have major impacts on the dominant modes of mass transfer.

Acknowledgment

Research funded by National Science Foundation award #123350.

Notation

$D_{1\text{eff}}$, $D_{2\text{eff}}$ = effective solid- and liquid-phase diffusivities, respectively, m^2/s
Φ_1, Φ_2 = potential in solid and electrolyte phases, respectively, V
R = gas constant, 8.414 J/mol/K
T = temperature (assumed constant at 298 K)
F = Faraday's constant, 96,485 C/mol
$k+$, $k-$ = reaction rate coefficient, positive, negative
t_+^*, t_-^* = cationic and anionic transport numbers, respectively
v^* = average molar velocity, m/s
c, c_+, c_- (c_i) = concentration of salt, anion, and cation in electrolyte, respectively, mol/m^3
α_a, α_c = apparent transfer coefficient in anode, cathode, respectively
a = interfacial area of electrode solid divided by the volume of the electrode, m^2/m^3
i_x = charge being transferred to/from solid from/to electrolyte in electrode in current per interfacial area, A/m^2
$K_{1\text{sep}}$ = solid-phase conductivity in separator, S
$\varepsilon_{1\text{sep}}$ = solid-phase porosity, separator
$\varepsilon_{2\text{sep}}$ = electrolyte phase porosity, separator
Br = Bruggeman coefficient (1.5)
i_2 = liquid-phase current density
i_1 = solid-phase current density
$\frac{d\ln(f\pm)}{d\ln(c)}$ = activity coefficient

Literature Cited

1. Suppes GJ, Sawyer BD, Gordon M. High-energy density flow battery validation. *AIChE J*. 2011;57(7):1961–1967.
2. Gordon M, Suppes G. Li-ion battery performance in a convection cell configuration. *AIChE J*. 2013;59(5):1774–1779.
3. Sawyer B, Suppes G, Gordon M, Heidlage M. Impact of electrode separator on performance of a zinc/alkaline/manganese dioxide packed-bed electrode flow battery. *J Appl Electrochem*. 2011;41(5): 543–550.
4. Li X, Zhang H, Mai Z, Zhang H, Vankelecom I. Ion exchange membranes for vanadium redox flow battery (VRB) applications. *Energy Environ Sci*. 2011;4(4):1147–1160.
5. Kear G, Shah AA, Walsh FC. Development of the all-vanadium redox flow battery for energy storage: a review of technological, financial and policy aspects. *Int J Energy Res*. 2012;36(11):1105–1120.
6. Weber A, Mench M, Meyers J, Ross P, Gostick J, Liu Q. Redox flow batteries: a review. *J Appl Electrochem*. 2011;41(10):1137–1164.
7. Gordon M, Suppes G. Convection battery—modeling, insight, and review. *AIChE J*. 2013;59:2833–2842.
8. Newman J, Tiedemann W. Porous-electrode theory with battery applications. *AIChE J*. 1975;21(1):25–41.
9. Doyle M, Fuller T, Newman J. Modeling of galvanostatic charge and discharge of the lithium/polymer/insertion cell. *J Electrochem Soc*. 1993;140(6):1526–1533.
10. Millikin M. "Univ. of Missouri team progressing with convection battery; enabling rechargeable lithium-metal batteries." Green Car Congress, 2013. http://www.greencarcongress.com/2013/05/suppes-20130514.html.
11. Newman J, Thomas-Alyea KE. *Electrochemical Systems, 3rd Edition*. Wiley: 2004. ISBN: 978-0-471-47756-3.
12. Park M, Zhang X, Chung M, Less GB, Sastry AM. A review of conduction phenomena in Li-ion batteries. *J Power Sources*. 2010; 195(24):7904–7929.
13. Doyle M, Newman J, Gozdz AS, Schmutz CN, Tamscon J-M. Comparison of modeling predictions with experimental data from plastic lithium ion cells. *J Electrochem Soc*. 1996;143(6):1890–1903.
14. Srinivasan V, Newman J. Discharge model for the lithium iron-phosphate electrode. *J Electrochem Soc*. 2004;151:A1517–A1529.
15. Fuller TF, Doyle M, Newman J. Simulation and optimization of the dual lithium ion insertion cell. *J Electrochem Soc*. 1994; 141(1):1–10.
16. Guduru A, Northrop PWC, Jain S, Crothers AC, Marchant TR, Subramanian VR. Analytical solution for electrolyte concentration distribution in lithium-ion batteries. *J Appl Electrochem*. DOI 10.1007/s10800-012-0394-4.
17. Daum P, Murray RW. Charge-transfer diffusion rates and activity relationships during oxidation and reduction of plasma-olymerized vinylferrocene films. *J Phys Chem*. 1981;85(4):389–396.
18. Sun G, Jin B, Sun G, Jin E, Gu H-B, Jiang Q. Characteristics of lithium iron phosphate mixed with nano-sized acetylene black for rechargeable lithium-ion batteries. *J Appl Electrochem*. 2011;41(1): 99–106.

Manuscript received Oct. 18, 2013, and revision received July 9, 2014.